

Revealing Pyrolysis Chemistry for Biofuels Production: Conversion of Cellulose to Furans and Small Oxygenates

Matthew S. Mettler^{†,††}, Samir H. Mushrif[†], Alex D. Paulsen^{††}, Ashay D. Javadekar[†],
Dionisios G. Vlachos[†], and Paul J. Dauenhauer^{††*}

[†] Department of Chemical Engineering and Catalysis Center for Energy Innovation,
University of Delaware, 150 Academy Street, Newark, DE 19716

^{††} Department of Chemical Engineering and Catalysis Center for Energy Innovation,
University of Massachusetts, 686 North Pleasant Street, Amherst, MA 01003

* To whom correspondence should be addressed. Email: dauenhauer@ecs.umass.edu

Electronic Supplementary Information

Design of Thin-Film Pyrolysis Experiments

Figure 2 in the main body of the paper uses dimensionless numbers to estimate the isothermal pyrolysis length scale limit as 20μm. In addition to this analysis, we have calculated transient temperature profiles in our thin-film as to determine the rate and uniformity by which biomass samples are heated. MATLAB⁴⁴ was used to solve the following transient, one-dimensional heat transport equation:

$$\frac{\partial T}{\partial t} = \frac{\lambda}{C_p \rho} \left(\frac{\partial^2 T}{\partial x^2} \right) + \frac{R \Delta H_{\text{rxn}}}{C_p \rho} \quad (1)$$

with boundary conditions,

$$\frac{\partial T}{\partial x}(x=0, t) = \frac{h_s(T-T_s)}{\lambda} \quad (2)$$

$$\frac{\partial T}{\partial x}(x=L, t) = \frac{h_a(T-T_a)}{\lambda} \quad (3)$$

$$T(x, t=0) = 25 \text{ }^{\circ}\text{C} \quad (4)$$

The values used in the model for cellulose physical properties (λ , C_p , ΔH_{rxn} and ρ ; taken from ¹⁴), reaction rates (R ; calculated from ⁶) and the solid-solid heat transfer coefficient (h_s ; intermediate value of 2000 W/m²-K based on previous work ^{2, 15}) are the same as those mentioned in the main body of the paper. The heat transfer coefficient between the thin-film and the ambient gas-phase (h_a) was assumed to be 20 W/m²-K. The characteristic length (L) is the cellulose thin-film thickness (i.e., 3 μm) which is determined from scanning electron microscopy (SEM). Using these parameters, thermal profiles for the cellulose thin-film were calculated.

Figure S1 shows the temperature as a function of position within the cellulose thin-film at several times. These profiles indicate that axial (i.e., along x-coordinate or thin-film thickness) temperature gradients within the thin-film are minor ($< 3 \text{ }^{\circ}\text{C}$) and that the cellulose sample is heated from ambient to reaction temperature in a few milliseconds, producing a temperature ramp greater than 1,000,000 $^{\circ}\text{C}/\text{min}$. This heat transfer time scale is 1-2 orders of magnitude faster than the time it takes for cellulose particles to volatilize in ablative pyrolysis reactors.² These simulations, coupled with the dimensionless analysis presented in the main paper, suggest that cellulose thin-films are heated isothermally and faster than pyrolysis reactions.

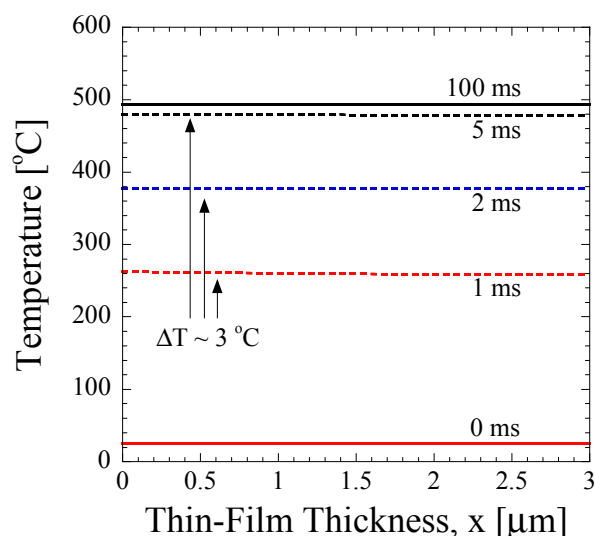


Figure S1. Transient temperature profiles for cellulose thin-film pyrolysis at 500 °C. One dimensional MATLAB simulations indicate that the cellulose thin-film is heated up to reaction temperature in approximately 5 milliseconds. In these calculations, an intermediate solid-to-solid heat transfer coefficient is assumed (2000 W/m²-K).^{2, 15} Cellulose physical properties are taken from previous work,¹⁴ and the thin-film thickness is assumed to be 3 μm as determined via SEM imaging.

In addition to fast heat transfer, the thin-film also allows unstable volatile products to diffuse through the reactive medium and escape to the gas-phase before they breakdown. To determine whether liquid-diffusion or pyrolysis chemistry is faster, the Damkohler Number (Da) is used to compare the ratio of diffusion ($\tau_{\text{diffusion}}$) and reaction (τ_{reaction}) timescales:

$$Da = \frac{\tau_{\text{diffusion}}}{\tau_{\text{reaction}}} = \frac{L^2 k}{D_A} \quad (5)$$

In (5), L is the characteristic length scale (e.g., thin-film thickness), k is the reaction rate (calculated from ⁶) and D_A is the liquid-phase diffusivity calculated using the semi-empirical Wilke-Chang method.⁴⁵ To calculate D_A , composition-dependent properties, such as molar volume, viscosity and molecular weight are needed. While previous work has shown that glucose monomers and dimers are present in the intermediate liquid,⁴⁶ a detailed description of the composition is unavailable. To obtain an order-of-magnitude estimate for the diffusion time scale within the intermediate liquid, we calculate high and low diffusivity estimates using two model

binary mixtures. The lower limit is calculated for a levoglucosan solute in a cellotriose solvent (slower diffusion) while the upper bound assumes water is diffusing through levoglucosan (faster diffusion). Using these estimates, reaction and liquid-phase diffusion timescales are calculated as a function of characteristic length. **Figure S2** shows that for pyrolysis at 500 °C, diffusion is much (i.e., one order-of-magnitude) faster than reaction for samples with characteristic length scales less than 70 μm . This calculation indicates that for typical cellulose particles (100-500 μm in size), liquid-phase diffusion is not substantially faster than reaction. In contrast, for the thin-films prepared in this work (3-10 μm in thickness), liquid-phase diffusion is much (i.e., 3-4 orders of magnitude) faster than pyrolysis reactions, as shown in **Figure S2**. The extreme difference between Damkohler numbers for thin-film and powder diffusion timescales arises from the fact that $\tau_{\text{diffusion}}$ is proportional to L^2 so small reductions in length scale result in much shorter diffusion times. This analysis indicates that thin-film pyrolysis allows primary pyrolysis products to escape to the gas-phase before they react.

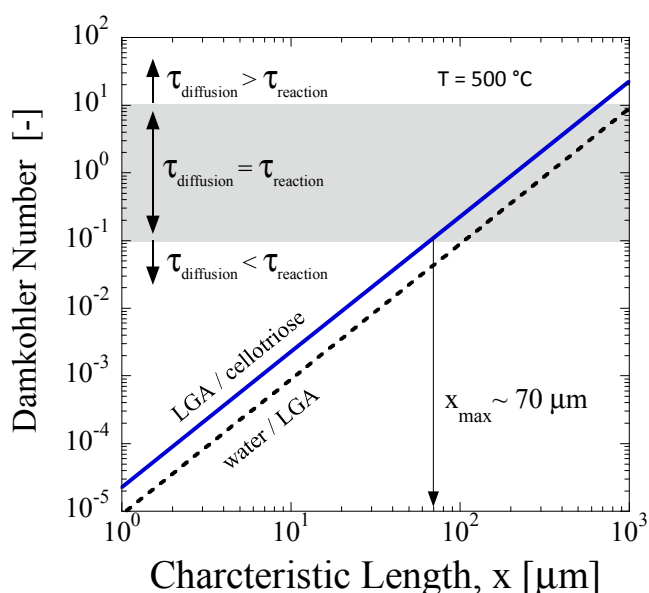


Figure S2. Damkohler number compares liquid-phase diffusion ($\tau_{\text{diffusion}}$) and reaction (τ_{reaction}) timescales as a function of characteristic length scale (x). Liquid-phase diffusivities are estimated using the Wilke-Chang relationship for two

model mixtures: levoglucosan (LGA) diffusing through cellotriose (LGA / cellotriose) and water diffusing through levoglucosan (water / LGA). For intrinsic kinetics, a film of less than 70 μm should be employed.

Cyclodextrins as a Class of Surrogates for Cellulose

Figure 3D in the main paper shows that α -cyclodextrin is largely representative of cellulose in flash pyrolysis. In the supplementary information, we provide additional material to further show α -cyclodextrin is an appropriate surrogate for cellulose and also evaluate two other commercially-available cyclodextrins: β - and γ -cyclodextrin.

In addition to α -cyclodextrin, two other commercially-available cyclodextrins were also compared to cellulose. **Figure S3** shows that β - and γ -cyclodextrin, like α -cyclodextrin, produce similar pyrolysis products to cellulose and are appropriate surrogates as well. While α -, β - and γ -cyclodextrin have a different number of glucose monomers (6, 7 and 8, respectively), they all have an end-group to monomer ratio of zero making them similar to cellulose in this respect (cellulose has an end-group to monomer ratio that is near zero: 0.01-0.0001). A key finding is that the end-group to monomer ratio is the most critical factor in identifying a surrogate.

In addition to primary products of flash pyrolysis, we have also compared cyclodextrins to cellulose using other traditional pyrolysis techniques. Thermogravimetric analysis (TGA) measures weight changes as samples are heated from ambient to reaction temperatures and has been used to study biomass pyrolysis in previous work.^{6,47} TA Instruments Q600 thermogravimetric analyzer (TGA) equipped with a 7-point balance (accurate to 0.0001 mg) was used to pyrolyze 10 mg biomass samples in an oxygen-free environment. Prior to pyrolysis, a 60 minute drying step was employed to remove volatiles (principally water) absorbed to biomass starting materials. Separately, this drying step was used to account for absorbed volatiles and close experimental carbon balances. Using this TGA technique, the temperature where pyrolysis reactions begin is determined for cellulose and cyclodextrins.

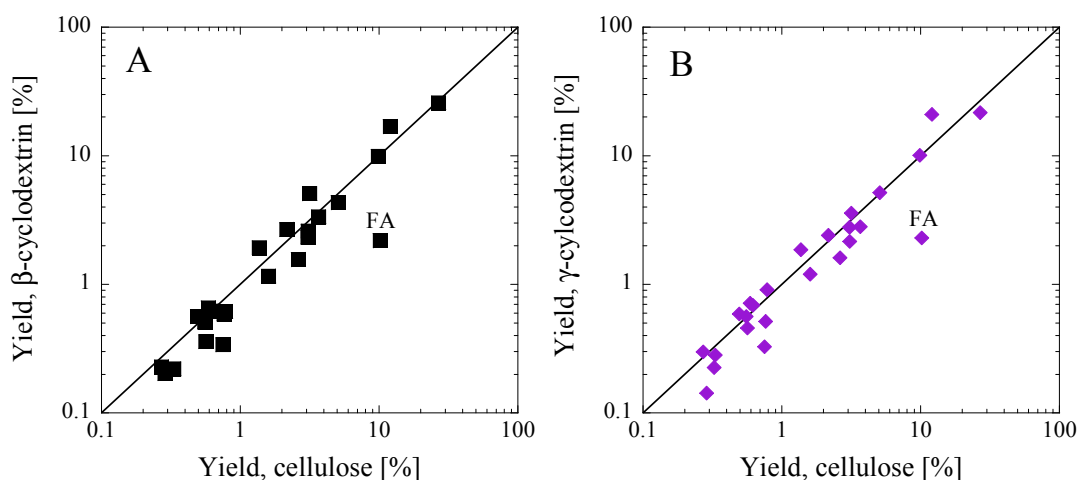


Figure S3. Comparison of major thin-film pyrolysis products of β -cyclodextrin (A) and γ -cyclodextrin (B) to cellulose at 500 °C. FA indicates formic acid.

Figure S4A shows that α -cyclodextrin has similar weight loss characteristics to cellulose for both slow (10 C/min) and fast (150 C/min) pyrolysis. While α -cyclodextrin appears to have a higher final mass compared to cellulose (i.e., more char production), the initial weight-loss temperature (i.e., 10% conversion), which indicates the onset of pyrolysis chemistry, occurs at nearly identical temperatures for cellulose and α -cyclodextrin in both slow (311 versus 312 °C) and fast (368 versus 371 °C) pyrolysis. In addition to α -cyclodextrin, TGA experiments were conducted to compare β - and γ -cyclodextrin to cellulose. **Figure S4B** shows that weight loss curves between α -, β - and γ -cyclodextrin and cellulose are also similar. All three cyclodextrins have similar initial weight-loss behavior compared to cellulose with 10% conversion occurring at 312, 320 and 313 °C for α -, β -, γ -cyclodextrin, respectively, vs. 311 °C for cellulose. The difference in final mass between cyclodextrins and cellulose could be a product of a different char-forming mechanism which is present with slower temperature ramps (10-150 °C/min) but not at the higher heating rates in powder and thin-film pyrolysis (>1,000,000 °C/min). These TGA results support

the finding of thin-film pyrolysis experiments, presented in the main body of the paper, that α -, β - and γ -cyclodextrin are very good surrogates for cellulose.

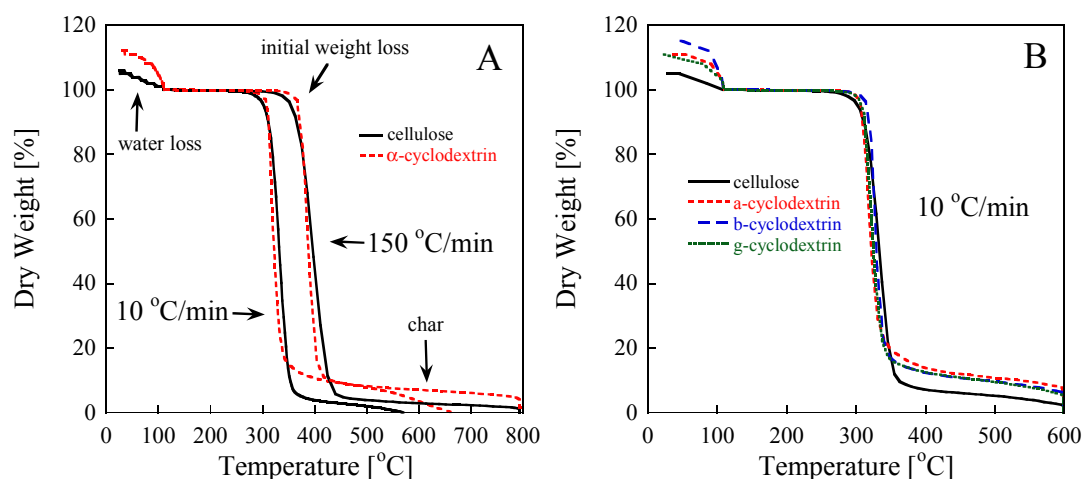


Figure S4. Comparison of cellulose to cyclodextrins (A and B) using thermogravimetric analysis. In A, weight-loss curves for α -cyclodextrin and cellulose are illustrated for slow (10 °C/min) and fast (150 °C/min) pyrolysis. For slow pyrolysis conditions (B), all cyclodextrins have similar behavior to cellulose. In each run, approximately 10mg of starting material was used.

***ab-initio* Molecular Dynamics**

The present article implements the Car-Parrinello molecular dynamics (CPMD) scheme¹⁷ to investigate the reaction mechanism of fast pyrolysis of α -cyclodextrin, a cellulose surrogate identified through our thin-film pyrolysis technique. Products obtained within the CPMD simulation timescale are shown in Figure S8. Furthermore, the origin of specific carbon atoms in the pyrolysis products, with respect to a single glucose unit of α -cyclodextrin molecule, is also shown. Detailed reaction mechanisms of the formation of furan ring and of glycolaldehyde and 2,3-hydroxy-succinaldehyde are discussed in Figure 4 of the main article. The mechanism of the formation of the five member furan ring from a glucose unit in α -cyclodextrin is representative of the mechanism in cellulose but differs from that of the furan ring formation mechanism from pure glucose. Bond dissociation energies of C-O, O-H, and C-C suggest that the thermolytic cleavage

of the O-H bond in the hydroxyl group attached to ^1C (in Figure S8) is unlikely (so as to give rise to the same furan ring formation mechanism in glucose) ahead of the C-C or ring C-O bond cleavage. Furthermore, our simulations show that all the products from α -cyclodextrin are formed through unimolecular decomposition of the molecule and that, in all the cases, the reaction is initiated by the cleavage of a glycosidic linkage between individual glucose units in the molecule. In the case of α -cyclodextrin, the reaction is initiated by the cleavage of a glycosidic linkage, whereas in glucose, it would be initiated with the ring opening of the molecule. This suggests that the reaction mechanism for generating the remaining pyrolysis products from glucose would also be different from that of α -cyclodextrin (or cellulose).

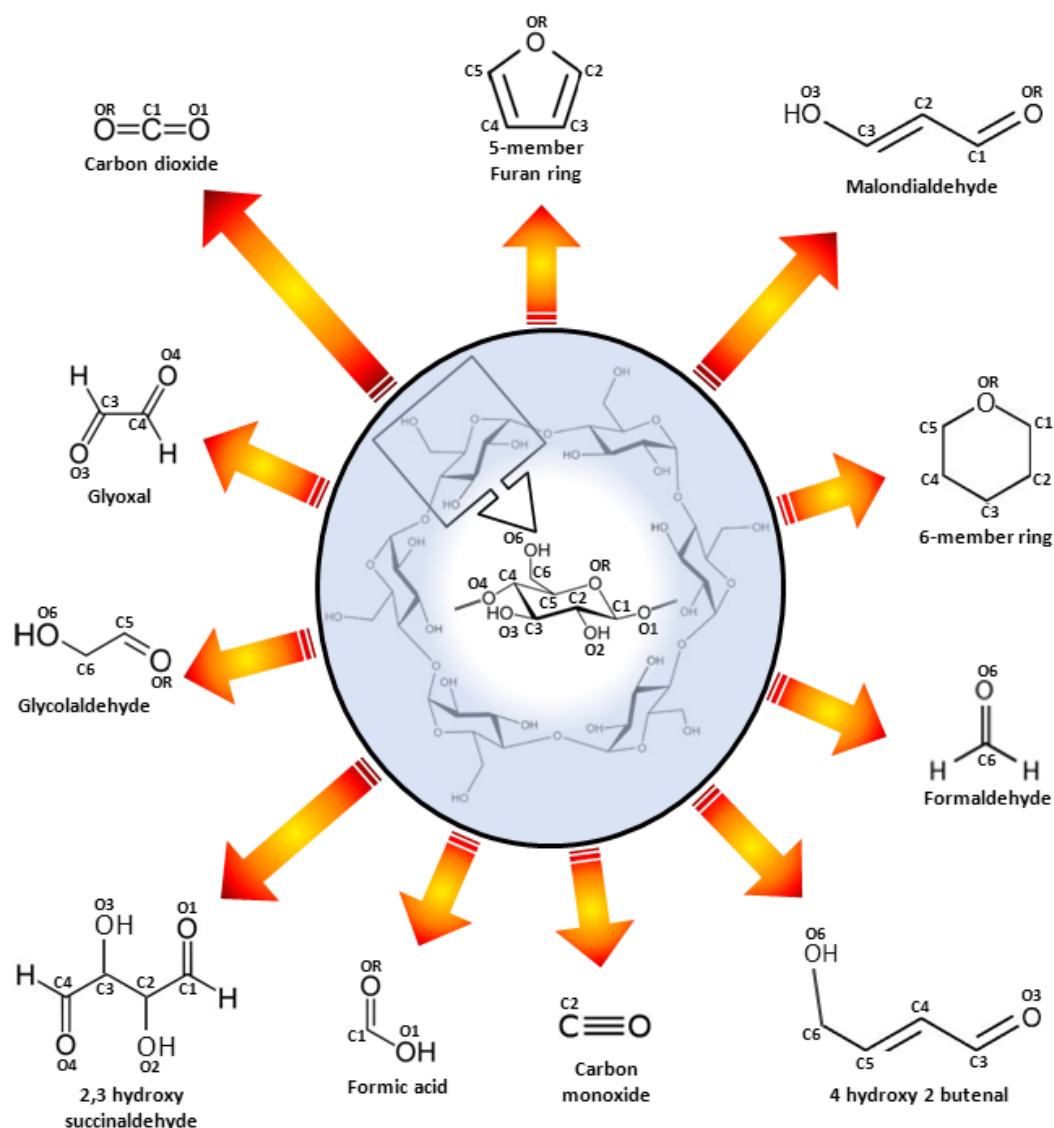


Figure S5. Products of pyrolysis of α -cyclodextrin from a CPMD simulation. The origin of carbon atoms in each product with respect to an individual glucose unit of α -cyclodextrin is also shown.

To investigate the nature of glycosidic bond cleavage (homolytic vs. heterolytic) in our simulations, we perform electron localization function (ELF analysis).³⁶ Silvi and Savin had proposed a topological analysis of the ELF to classify chemical bonds as covalent or ionic.³⁷ Kohout and Savin also provided a method to calculate the ELF separately for each spin density.⁴⁸ Spin dependent ELF calculations provide information about the localization of unpaired electrons

(e.g., the unpaired electron in free radical species). Consequently, Melin and Fuentealba analyzed the α - and β -spin contributions to ELF separately to study the localization of unpaired electrons in methyl and phenyl radicals.⁴⁹ Inspection of the localization domain, the spatial region bounded by a closed ELF isosurface, also provides insight into the electronic structure. At low values of the ELF, there is only one localization domain, containing all the attractors (local maxima). As the ELF value is increased, the localization domain splits into a number of irreducible and reducible domains, containing one and multiple attractors, respectively, until all the domains become irreducible. The reduction of the reducible localization domains gives rise to distinguishable valence basins. The synaptic order of a valence basin, i.e., the number of atomic core basins in contact with the valence basin, is also used to characterize the chemical interaction as electron-sharing or non-electron-sharing.

The ELF was computed on snapshot geometries taken directly from our CPMD simulation trajectory. Single point calculation (with a spin multiplicity check) was performed on each structure before computing the ELF. Snapshot molecular structures picked from the CPMD trajectory of the pyrolysis reaction of α -cyclodextrin to furan and the corresponding ELF isosurfaces are shown in **Figure S6**. For an initial glucose unit before the reaction and for the final furan ring, only the total ELF isosurfaces are shown. For the intermediate species, both α - and β -spin ELF isosurfaces are shown separately. Topology of the ELF- β basin for oxygen atom ^1O is significantly different from that of the ELF- α basin. The topology of the ELF- α basin is similar to that of the ELF basin for lone pair of electrons of the oxygen atom, whereas a toroidal basin can be seen for the localization of the β -spin electron. This suggests the presence of an unpaired β -spin electron in oxygen atom ^1O . Localization of the unpaired electron in a toroidal basin whose plane is at right angle to the $^1\text{C}-^1\text{O}$ bond would minimize its repulsion with the bonding and lone pair electrons of the oxygen atom. Similarly, as highlighted in the blue contour, an additional localization region can be seen in the ELF- β isosurface in the vicinity of the carbon atom of the

cleaved glycosidic linkage. This confirms the presence of an unpaired β -spin electron in the carbon atom. It thus suggests that the first glycosidic bond scission in the α -cyclodextrin to furan reaction occurs homolytically. It has to be noted that the lowest energy spin state of the structure was found to be of multiplicity 3 (and not 1). Similarly, ELF analysis was also performed to investigate the ring opening and dehydration steps in the reaction; it was found that both these bond cleavages are also homolytic. The radical intermediates shown in **Figure S6** are extremely short-lived, since the entire timescale of the reaction, starting from the glycosidic bond cleavage to the formation of the furan ring, is around 0.2 ps. It is possible that these short-lived radical species seen during the dynamics of the reaction do not exist long enough to be considered “radical intermediates”, but are continuously evolving structures during the rearrangement of the bonding pattern in the glucose unit, after the glycosidic bond cleavage.

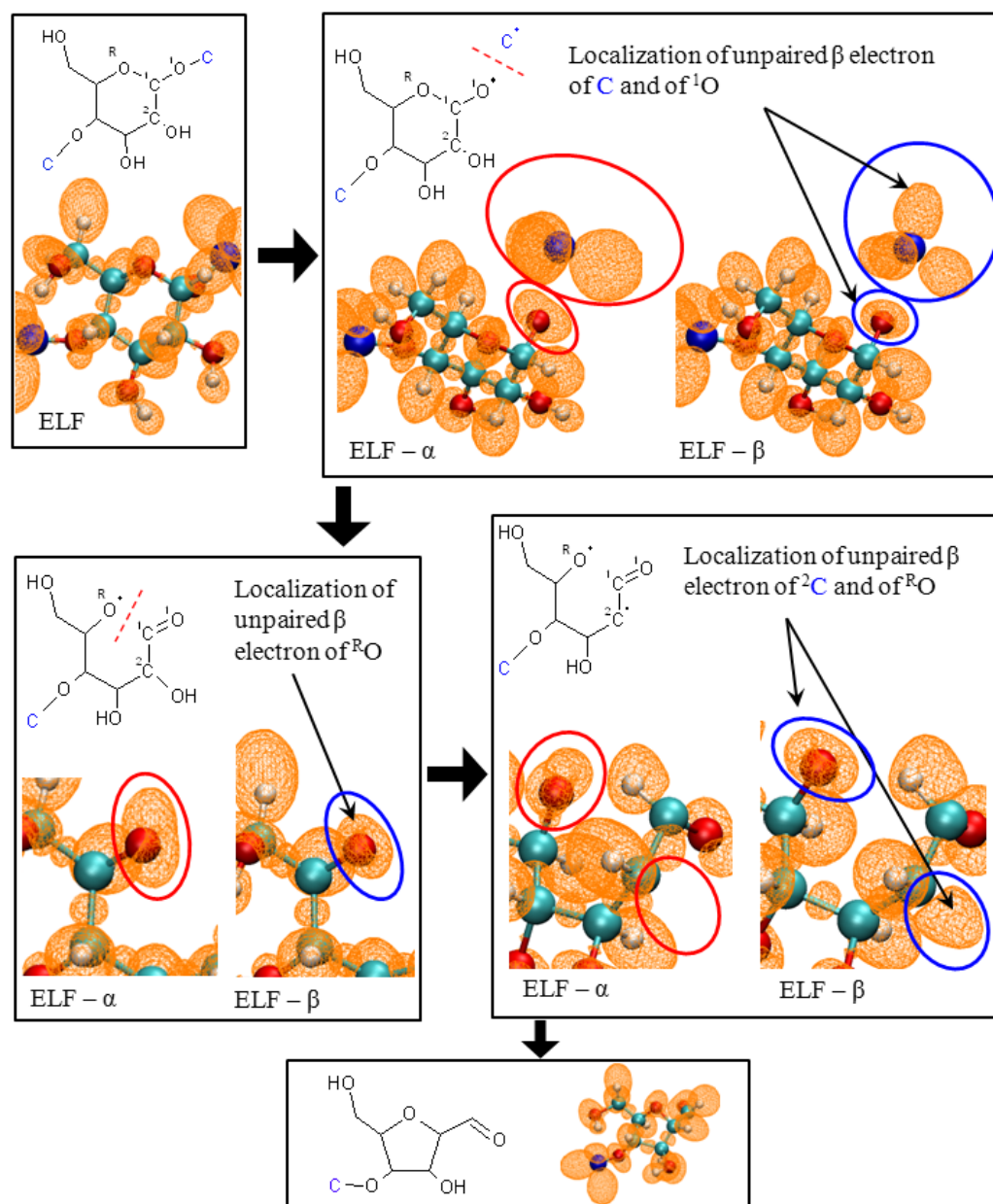


Figure S6. Snapshot structures along the CPMD trajectory of α -cyclodextrin to furan and the corresponding ELF isosurfaces at an isovalue of ~ 0.8 . Separate ELF- α and ELF- β isosurfaces are shown only for the radical species.

Characterization of Starting Materials

For the starting materials studied in Figure 3A-F of the main paper (i.e., glucose, cellulose, α -cyclodextrin, etc.), volatile and non-volatile impurities were quantified. To determine the mass of adsorbed volatiles, a TA Instruments Q600 thermogravimetric analyzer (TGA) was used. **Table S1** shows that glucose has relatively little adsorbed volatiles (0.3%), while a substantial amount of volatiles are adsorbed in cellulose (5.5%), cellohexaose (9.9 %) and α -cyclodextrin (10.6 %). We speculate that these adsorbates consist principally of water, but mass spectrometry is needed to confirm this hypothesis. The volatile content determined with TGA allows us to properly close the carbon balance for the data presented in Figure 3A-D of the main paper.

In addition to quantifying adsorbates, we also characterized non-volatile impurities using a Waters 2695 liquid chromatography systems equipped with a Hi-Plex Na 10 μ m column. **Table S1** shows that while glucose contains relatively little non-volatile impurities, both cellohexaose and α -cyclodextrin starting materials contain moderate amounts. Cellulose could not be separated from impurities using this column so we cannot comment on non-volatile content of this starting material. In the case of α -cyclodextrin, a single impurity was observed that did not match any of the tested standards (i.e., those listed in **Table S1** and cellobiose, cellotriose, cellotetraose, cellopentaose, maltose, maltotriose, maltotetraose, maltopentaose, maltohexaose). Impurities for cellohexaose were much easier to identify since it is well-known that cellohexaose preparation techniques produce a distribution of cellodextrins rather than a single product.⁵⁰ In our cellohexaose starting material we find minor amounts of cellopentaose (confirmed by retention-time analysis), celloheptaose (not confirmed by retention-time analysis) and celloctaose (not confirmed by retention-time analysis). While pure samples for celloheptaose and celloctaose were not available, previous work has shown that these compounds are present in cellohexaose preparation and that their retention time is near that of cellohexaose.⁵⁰ These non-volatile

impurities are a source of error in our experiments, but since they are chemically similar to the pure component and make up a relatively minor fraction of the overall starting material (8.2% for cellohexaose and 3% for α -cyclodextrin), we make no modification to the results presented in Figure 3C-D.

Table S1. Adsorbed volatile content and non-volatile impurities for starting materials used in thin-film experiments.

	Adsorbed Volatiles [%]	Non-volatile Impurities (name) [%]
Glucose	0.3	0
Cellohexaose	9.9	3.9 (cellopentaose) 2.8 (celloheptaose)* 1.5 (cellooctaose)*
Cellulose	5.5	N/A
α-cyclodextrin	10.6	3 (unknown)

* Compounds not confirmed via retention time since pure standards are unavailable.

Preparation and Characterization of Thin-Films

Thin-films were prepared by creating a 1wt% solution (or in the case of cellulose, a suspension) of carbohydrates and water and then depositing 25 μ L of the solution into a 4 x 8mm (diameter x height) cylindrical, deactivated stainless steel pyrolysis crucible. Excess water was then removed by applying a -20 inHg vacuum at 35 °C for approximately two hours.

Figure 2 in the main part of the paper shows a scanning electron microscopy (SEM) image of a cellulose thin-film. Scanning electron microscopy images were acquired using JEOL 7400F. The samples were mounted on aluminum stubs using carbon tape. The microscope enabled imaging of the cellulose thin film formed inside the metal cups without much charging or film damage, at accelerating voltage of 2 kV. The samples of cellulose particles were coated with carbon before imaging to avoid charging, and the images were acquired at an accelerating voltage of 3 kV.

In the supplemental section we present additional SEM images to confirm the microscale dimensions of our thin-films. While cellulose thin-films could be easily removed from the pyrolysis crucible without damaging the sample, α -cyclodextrin adhered strongly to the crucible wall and therefore had to be characterized while bound to the reaction vessel wall. **Figure S7** shows that cellulose (top row) thin-films are 1-3 μm in thickness while α -cyclodextrin samples (bottom row) have a characteristic dimension of approximately 10 μm . These dimensions are below the isothermal (20 μm) and well-mixed (70 μm) limits outlined in Figure 2 (main paper) and **Figure S2**, respectively.

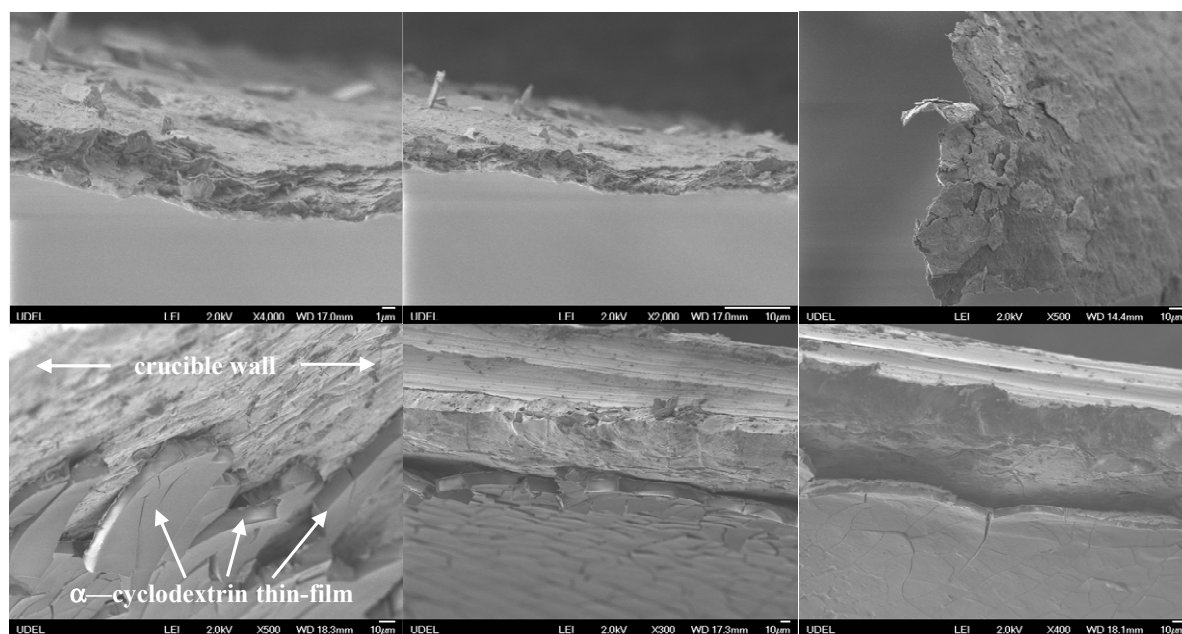


Figure S7. Scanning electron microscopy (SEM) images of cellulose (top row) and α -cyclodextrin (bottom row) thin-films. Cellulose thin-films were removed from the pyrolysis crucible prior to imaging while α -cyclodextrin films were imaged while still adhering to the crucible.

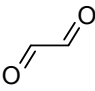
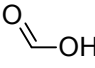
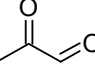
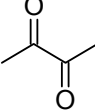
Identification of Pyrolysis Products

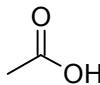
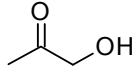
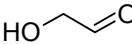
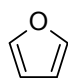
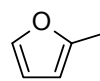
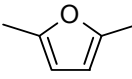
Figure 3A-F in the main paper shows the yield of identified pyrolysis products. In the supplemental section of the paper, we present a summary of the methods used to identify these products. Compounds were identified through gas chromatography retention time analysis, mass spectroscopy and by comparison to pyrolysis products reported in previous work. Many compounds, such as furan, levoglucosan, and glycolaldehyde, are straightforward to identify since they have been reported in previous work,^{29, 34} produce a clean mass spectrum that compares favorably to established benchmarks and are commercially available. While identification is easy for some pyrolysis products, other analytes are more challenging since one or more of these characterization methods is unavailable. One major component which was challenging to identify is methyl glyoxal. Table S2 shows that methyl glyoxal can be up to six percent of the total product yield, and, to our knowledge, this analyte has not been identified in previous work. The mass spectrum for the analyte (methyl glyoxal) has three major ions: 72, 56 and 44 mass-to-charge ratio (m/z) with the parent ion (72) indicating the molecular weight. Because of the atomic composition of the biomass starting material, this compound can only contain carbon, hydrogen, and oxygen and the chemical formula must be $C_3H_4O_2$ or $C_4H_8O_2$. The response at 56 m/z likely corresponds to a loss of an oxygen atom (-16 Daltons) while the 44 ion is probably due to a loss of a CO (-28 Daltons). From these ions, it was deduced that the analyte likely has at least one carbonyl group. With an early retention time of 10.5 minutes, the analyte eluted in the range of linear oxygenates. Because all other identified linear oxygenates contained two oxygen atoms, we hypothesized that the unknown compound is a straight chain oxygenate with the formula $C_3H_4O_2$. Using the NIST Mass Spectral Library, compounds with formulas $C_3H_4O_2$ and $C_4H_8O_2$ were examined to find possible matches to the unknown compound. From this analysis, a list of possible chemicals was constructed. After testing all compounds on the list, we found that methyl glyoxal had a retention time identical to the analyte. Further evidence is that the mass spectrum

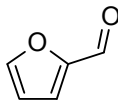
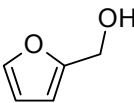
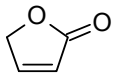
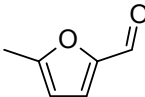
for pure methyl glyoxal contains the same major mass spectra ions (72, 56, and 44) as the analyte. Based on this information, the unknown peak at 10.5 minutes was assigned to methyl glyoxal. Not all compounds are commercially available for retention time testing and therefore identification relied on mass spectrometry. Three compounds, as indicated in Table S2, were identified through the use of mass spectrometry only. Of these three, two had been identified in previous work: 1,6-anhydroglucopyranose (AGP) and 1,4;3,6-dianhydro- α -D-glucopyranose (DGP).^{29, 34} These compounds were easily confirmed with our mass spectrometer. The third compound (retention time of 44.6 minutes), which to our knowledge has not been reported in previous work, was identified using Mass Spectrometry as 1,2-cyclopentanedione (CPD). The mass spectra for this analyte contained several ions which can easily be produced by CPD fragmentation. The loss of a CHO from CPD results in an ion of 69 Daltons, which we observe. We also observe an ion of 55 Daltons, which could be produced from the loss of a C₂H₃O. Furthermore, the NIST library search program presented CPD as a strong match for the unknown peak over six separate pyrolysis runs. Finally, CPD has a similar structure to 2-hydroxy-3-methyl-2-cyclopenten-1-one (CPD has one less methyl group), a pyrolysis product identified via mass spectrometry and retention time analysis. Based on this evidence, we identify this analyte as CPD. One peak was identified without a strong NIST Mass Spectral Library match or a retention time comparison. This peak, shown in Table S2 (retention time of 69.0 minutes), produces no exact match to the NIST library but analysis of the mass spectra indicates that the analyte has a molecular weight of 144. Additionally, responses were observed at 126, 113, 97, 87, 69, and 57 m/z. Shafizadeh and co-workers identify a major product from cellulose pyrolysis as 1,5-anhydro-4-deoxy-D-glycero-hex-1-en-3-ulose (ADGH) using a combination of techniques (H-NMR, IR spectrometry, UV spectrometry, and mass spectrometry).³⁴ Shafizadeh and co-workers show that ADGH has a molecular weight of 144 Daltons and elutes between levoglucosan and 1,4;3,6-dianhydro- α -D-glucopyranose. ADGH is a six member ring that is similar to glucose except that

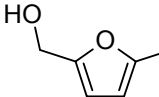
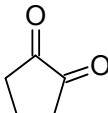
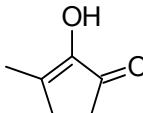
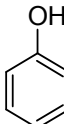
two water molecules (-36 Daltons) have been removed via dehydration. In our mass spectrometry measurements, we observe several ions which can easily be produced from ADGH fragmentation. From ADGH, the loss of a CH_3O results in an ion of 113 Daltons (which we observe). The loss of a CH_3O and an oxygen results in an ion of 97 Daltons, which we also observe. Finally, we observe an ion of 126 Daltons, which could be produced by ADGH dehydration ($-\text{H}_2\text{O}$). The analytes' retention time relative to levoglucosan and 1,4;3,6-dianhydro- α -D-glucopyranose (DGP), coupled with analysis of the mass spectra and the previous work of Shafizadeh, indicates that our analyte is ADGH.

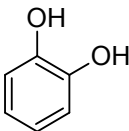
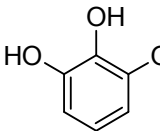
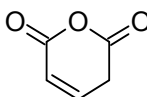
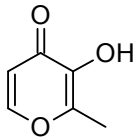
Table S2. Summary of identified pyrolysis products in powder and/or thin film pyrolysis experiments at 500 °C.

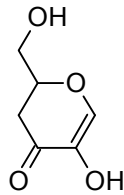
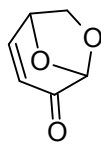
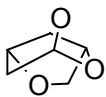
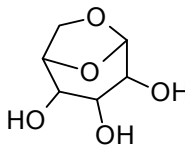
Compound	Structure	Ref.	Retention Time [min]	Molar Mass	Major Ion Fragments			Percent Yield (Carbon Basis)
light gasses								
carbon monoxide	$\text{C}\equiv\text{O}$	-	3.302	28				0– 5.6
carbon dioxide	$\text{O}=\text{C}=\text{O}$	-	13.162	44				0.4 – 6.8
linear oxygenates								
glyoxal		-	5.99	58	Ion	Relative Height	Fragment Lost	0 – 0.2
					58	999	—	
					56	845	- H ₂ (-2)	
formic acid		29	15.287	46	Ion	Relative Height	Fragment Lost	0.2 – 13.7
					46	999	—	
					45	753	- H (-1)	
methylglyoxal		-	10.469	72	Ion	Relative Height	Fragment Lost	1.0 – 6.0
					72	999	—	
					56	389	- O (-16)	
					44	487	- CO (-28)	
2,3 butanedione		-	17.011	86	Ion	Relative Height	Fragment Lost	0.1 – 1.3
					86	999	—	

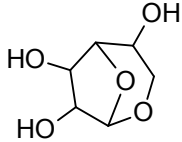
acetic acid		29	19.172	60	Ion	Relative Height	Fragment Lost	0.1 – 0.6
					60	734	—	
					45	999	-CH ₃ (-15)	
hydroxyacetone		29	23.143	74	Ion	Relative Height	Fragment Lost	0 – 2.9
					74	999	—	
					45	293	CHO (-29)	
glycoaldehyde		29	53.334	60	Ion	Relative Height	Fragment Lost	0 – 11.5
					60	999	—	
					58	290	- H ₂ (-2)	
					56	157	- H ₄ (-4)	
Furans								
furan		29	10.355	68	Ion	Relative Height	Fragment Lost	0 – 0.6
					68	999	—	
2-methyl furan		29	17.929	82	Ion	Relative Height	Fragment Lost	0.2 – 0.7
					82	999	—	
					81	589	- H (-1)	
					53	613	-CHO (-29)	
2,5 dimethyl furan		-	26.476	96	Ion	Relative Height	Fragment Lost	0.2 – 1.1
					96	999	—	
					95	946	- H (-1)	
					81	326	-CH ₃ (-15)	
					53	553	- C ₂ H ₃ O (-43)	

furfural		29	36.775	96	Ion	Relative Height	Fragm ent Lost	0.7 – 2.4
					96	999	—	
					95	953	- H (-1)	
2-furanmethanol		29	38.973	98	Ion	Relative Height	Fragm ent Lost	0.5 – 1.3
					98	999	—	
					97	614	- H (-1)	
					81	747	-OH (-17)	
					69	553	-CHO (-29)	
					53	796	(-45) ^β	
2(5H) furanone			43.588	84	Ion	Relative Height	Fragm ent Lost	0.1 – 0.7
					84	507	—	
					55	999	-CHO (-29)	
					54	267	-CH ₂ O (-30)	
5-methyl furfural		29	47.875	110	Ion	Relative Height	Fragm ent Lost	0.3 – 0.7
					110	999	—	
					109	814	- H (-1)	
					57	470	(-53) ^β	
					55	389	(-55) ^β	
					53	608	(-57) ^β	

5-hydroxymethyl-furfural (HMF)		29, 34	64.238	126	Ion	Relative Height	Fragment Lost	2.1 – 4.1
					126	593	—	
					125	99	- H (-1)	
					97	999	-CHO (-29)	
					69	327	(-57) ^β	
					53	194	(-73) ^β	
cyclopentanes								
1,2-cyclopentanone ^γ		-	44.636	98	Ion	Relative Height	Fragment Lost	0.1 – 0.8
					98	999	—	
					69	300	-CHO (-29)	
					55	655	- C ₂ H ₃ O (-43)	
2-cyclopenten-1-one, 2-hydroxy-3-methyl		29	52.209	112	Ion	Relative Height	Fragment Lost	0.1 – 0.4
					112	999	—	
					83	291	-CHO (-29)	
					69	481	- C ₂ H ₃ O (-43)	
					55	473	(-57) ^β	
aromatics								
phenol			49.222	94	Ion	Relative Height	Fragment Lost	0 ^α
					94	999	—	
					66	352	-CO (-28)	
					65	226	-CHO (-29)	

catechol			62.387	110	Ion	Relative Height	Fragm ent Lost	0.1 – 0.9
					110	999	—	
					92	111	-H ₂ O (-18)	
					81	132	-CHO (-29)	
					64	299	(-46) ^B	
pyrogallol			71.701	126	Ion	Relative Height	Fragm ent Lost	0 ^a
					126	999	—	
					108	259	H ₂ O (- 18)	
					80	305	(-46) ^B	
					52	285	(-74) ^B	
pyrans								
2H-pyran- 2,6(3H)- dione ⁷		-	49.915	112	Ion	Relative Height	Fragm ent Lost	0 ^a
					112	690	—	
					84	707	-CO (- 28)	
					56	279	(-56) ^B	
					55	999	(-57) ^B	
maltol		-	57.544	126	Ion	Relative Height	Fragm ent Lost	0 – 0.6
					126	999	—	
					97	196	-CHO (-29)	
					71	360	(-55) ^B	
					55	204	(-71) ^B	

1,5-anhydro-4-deoxy-D-glycero-hex-1-en-3-ulose ^δ		34	69.000	144	Ion	Relative Height	Fragment Lost	0 – 5.5
					144	846	—	
					113	217	-CH ₃ O (-31)	
					97	678	(-47) ^β	
					87	999	(-57) ^β	
					69	384	(-75) ^β	
					57	576	(-87) ^β	
anhydrosugars								
levoglucosene		29	57.889	126	Ion	Relative Height	Fragment Lost	0.1 – 3.0
					98	259	-CO (-28)	
					68	999	(-58) ^β	
					53	946	(-73) ^β	
					51	430	(-75) ^β	
					50	588	(-76) ^β	
1,4;3,6-dianhydro-α-D-glucopyranose ^γ		29, 34	63.373	144	Ion	Relative Height	Fragment Lost	0.4 – 2.9
					144	—	—	
					114	286	-C ₂ HO (-30)	
					70	269	(-74) ^β	
					69	999	(-75) ^β	
					57	453	(-87) ^β	
levoglucosan		29, 34	75.158	162	Ion	Relative Height	Fragment Lost	3 – 56.6
					144	—	-H ₂ O (-18)	
					73	362	(-89) ^β	
					60	999	(102) ^β	
					57	427	(105) ^β	

1,6 Anhydrogluco furanose ^γ		29, 34	77.375	162	Ion	Relative Height	Fragm ent Lost	0.4 – 6.7
					73	999	(-89) ^β	
					69	309	(-93) ^β	
					61	208	(-101) β	
					45	209	(-117) β	